jem00 | ACSJCA | JCA11.1.4300/W Library-x64 | research.3f (R4.1.i3 HF01:4938 | 2.1) 2018/08/24 11:08:00 | PROD-WS-116 | rq_4438989 | 7/05/2019 12:43:01 | 7 | JCA-DEFAULT

NANO LETTERS

Letter

pubs.acs.org/NanoLett

Evidence for Helical Hinge Zero Modes in an Fe-Based Superconductor

Mason J. Gray,[†] Josef Freudenstein,[†] Shu Yang F. Zhao,[‡] Ryan O'Connor,[†] Samuel Jenkins,[†] Narendra Kumar,[†] Marcel Hoek,[†] Abigail Kopec,[†] Soonsang Huh,[§] Takashi Taniguchi,[∥] Kenji Watanabe,[∥] Ruidan Zhong,[⊥] Changyoung Kim,[§] G. D. Gu,[⊥] and K. S. Burch[*,†]

[†]Department of Physics, Boston College, Chestnut Hill, Massachusetts 02467, United States

[‡]Department of Physics, Harvard University, Cambridge, Massachusetts 02138, United States

[§]Department of Physics and Astronomy, Seoul National University (SNU), Seoul 08826, Republic of Korea

[∥]National Institute for Materials Science, 1-1 Namiki, Tsukuba 306-0044, Japan

[⊥]Condensed Matter Physics and Materials Science Department, Brookhaven National Laboratory, Upton, New York 11973, United States

Supporting Information

ABSTRACT: Combining topology and superconductivity provides a powerful tool for investigating fundamental physics as well as a route to fault-tolerant quantum computing. There is mounting evidence that the Fe-based superconductor $FeTe_{0.55}Se_{0.45}$ (FTS) may also be topologically nontrivial. Should the superconducting order be $s^{\pm}$, then FTS could be a higher order topological superconductor with helical hinge zero modes (HHZMs). To test the presence of these modes, we have fabricated normal-metal/superconductor junctions on different surfaces via 2D atomic crystal heterostructures. As expected, junctions in contact with the hinge reveal a sharp zero bias anomaly that is absent when tunneling purely into the *c*-axis. Additionally, the shape and suppression with temperature are consistent with highly coherent modes along the hinge and are incongruous with other origins of zero bias anomalies. Furthermore, additional measurements with soft-point contacts in bulk samples with various Fe interstitial contents demonstrate the intrinsic nature of the observed mode. Thus, we provide evidence that FTS is indeed a higher order topological superconductor.

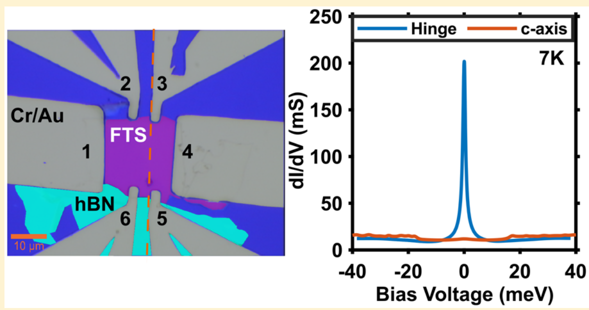

KEYWORDS: *Higher order topology, 2D superconductor, hinge modes, Andreev reflection*

New particles can be a convincing signature of emergent phases of matter, from spinons in quantum spin liquids[1] to the Fermi arcs of Weyl semimetals.[2,3] Beyond potentially indicating a broken symmetry or topological invariant, they can be put to use in future topological quantum computers.[4] Until recently, it was believed the nontrivial topology of the bulk would lead to new states in one lower dimension at the boundary with a system of differing topology. However, higher order topological insulators (HOTIs) have been realized,[5−10] where the resulting boundary modes exist only at the intersection of two or more edges, producing 1D hinge or 0D bound states. One route to creating these higher order states is through the combination of a topological insulator and a superconductor with anisotropic pairing.[11−14] Usually, this is done by combining two separate materials and inducing superconductivity into the TI via proximity.[15−19] However, this method requires long coherence lengths and extremely clean interfaces, making experimental realization of devices quite difficult. For studying HOTI, as well as the combination of strong correlations and topology, the material $FeTe_{0.55}Se_{0.45}$ (FTS) may be ideal, as it is a bulk, high temperature superconductor with anisotropic pairing that also hosts topologically nontrivial surface states.[20−22]

FTS is part of the $FeTe_{1-x}Se_x$ family of Fe-based superconductors, which ranges from an antiferromagnet in FeTe to a bulk superconductor in FeSe.[23] These generally have the same fermiology as the other Fe-based superconductors in that there are hole pockets at the Γ-point and electron pockets at the M-points.[20,24−27] The relative strengths of the interband vs intraband scattering in principle should determine the superconducting symmetry; however, there is a complex interplay between the spin-fluctuation exchange, intraband Coulomb repulsion, and doping level that all contribute to the symmetry of the superconducting order parameter.[28,29] Indeed, experiments performed on $FeTe_{0.55}Se_{0.45}$ find no evidence for a

Received: February 26, 2019
Revised: June 28, 2019
Published: July 3, 2019

DOI: 10.1021/acs.nanolett.9b00844
Nano Lett. XXXX, XXX, XXX−XXX

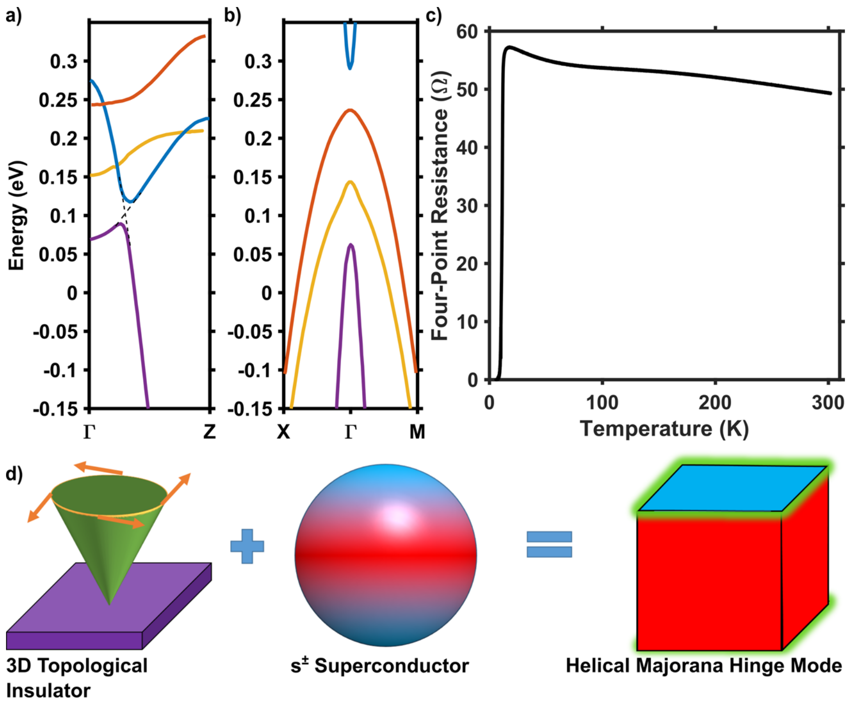

Figure 1. Theoretical band structure of $FeTe_{0.55}Se_{0.45}$ along (a) the Γ−*Z* and (b) the *X*−Γ−*M* cuts.[21] The p_z-orbital of the chalcogenide is shown in blue, crossing the three d-orbitals, resulting in two Dirac points and topological, spin−orbit gap. (c) Resistance vs temperature graph for an exfoliated flake of FTS, showing a clear superconducting transition around 10 K. (d) Diagram showing the ingredients needed for a helical Majorana hinge mode.

node with strong signatures of $s^{\pm}$ order,[25,26,30] while experiments on other alloys suggest nodal $s^{\pm}$, anisotropic s-wave, and even p-wave.[27,31−34] Interestingly, tuning away from FeSe leads to enhanced spin−orbit coupling and bandwidth. As a result, the p-orbital is shifted down in energy, crossing the d-orbitals with opposite parity along the Γ to *Z* direction (see Figure 1a and b). The first two crossings are protected by crystalline symmetry resulting in bulk Dirac states above the Fermi energy. However, the lowest energy crossing is avoided, resulting in a spin−orbit coupled gap, resembling those typically found in topological insulators.[21,35] While the Fermi level falls into this gap, the original hole and electron Fermi surfaces at Γ and *M*, respectively, are retained.[20,21] ARPES measurements have observed the resulting spin-momentum locked surface states, as well as their gaping out in the superconducting state.[20,36] Additionally, there is evidence from STM that this results in apparent Majorana zero modes inside magnetic vortices.[22,37,38]

Recent theoretical work on FTS has suggested that the combination of an $s^{\pm}$ order parameter and topological surface states could give rise to higher order topological superconductivity.[12] In short, the changing superconducting phase causes the surface states to gap out anisotropically. Depending on the relative strength of the isotropic versus anisotropic term, this could lead to the [001] and the [100] or [010] face having superconducting order parameters with opposite phase. As shown in Figure 1d, this is predicted to produce a pair of 1D helical Majorana hinge modes emerging at the 1D interface of the top/side surfaces.[12] Whether or not the modes we observe are indeed Majorana modes, the appearance of HHZM requires both $s^{\pm}$ superconductivity as well as strong 3D TI surface states. Thus, observing helical hinge zero modes in FTS would provide strong evidence that it is an $s^{\pm}$ topological superconductor.

To search for the HHZM, it is tempting to rely on methods previously exploited to reveal the unconventional nature of the cuprates.[39] Specifically, normal-metal/superconductor junctions demonstrated Andreev bound states resulting from the d-wave order only on [110] surfaces.[19,40−42] In the case of FTS, this approach is more challenging, as one must tunnel into the hinge between [001] and [010] and the modes are nominally charge neutral, thus requiring an Andreev process to be observed.[43] To achieve this, we created 2D atomic crystal heterostructures with thick hBN covering half of the FTS. By draping contacts over the side of the FTS or atop the hBN, we can separately probe conductance into the hinge from the *c*-axis. As expected for modes protected from backscattering, we find a cusp-like zero bias peak only on the hinge contacts that is absent from the *c*-axis junctions. The mode is well-described by a Lorentzian, consistent with other studies on one-dimensional zero energy bound states.[44] Confirmation that the mode does not result from our fabrication method or defect density is provided by soft-point contact measurements on facets of various bulk crystals (see Figure S3). Taken together, these data strongly suggest the presence of the HHZM in FTS resulting from its higher order topological nature and the presence of $s^{\pm}$ superconductivity.[19,45] The helical hinge zero mode in FTS should only exist in the superconducting state. As such, we expect a sharp zero bias conductance feature below T_c on the hinges between the [001] and side surfaces as compared to purely on the [001] face. Alternatively, Majorana zero modes on the hinge should give quantized conductance, revealed through nearly perfect Andreev reflection.[12] However, as discussed later, observing this quantized conductance may be challenging, as the coherence length in FTS is ≈3 nm.[33,34] To test this, we used 2D atomic crystal heterostructures to simultaneously fabricate normal-metal/superconductor (NS) low barrier junctions on

DOI: 10.1021/acs.nanolett.9b00844
Nano Lett. XXXX, XXX, XXX−XXX

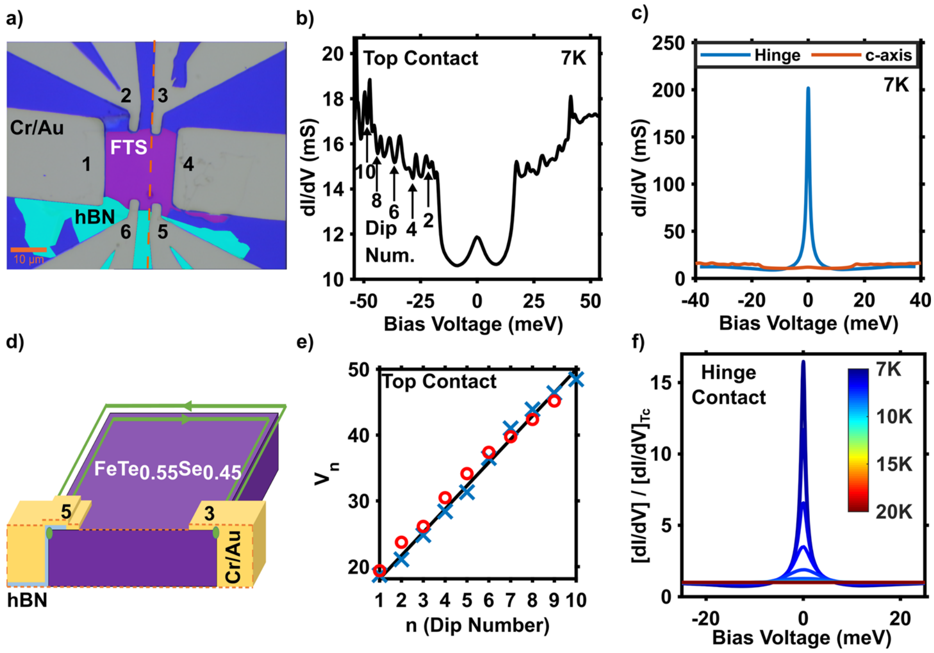

Figure 2. (a) False color image of the exfoliated device; numbers denote contacts used. (b) $\frac{dI}{dV}$ vs DC bias voltage for contact 5 at 7 K. (c) $\frac{dI}{dV}$ vs DC bias voltage for contact 3 at 7 K. (d) Depiction of contact geometry for top only (5) and hinge (3) contacts. (e) Dip number vs voltage for *c*-axis only contacts. The black line is a fit to McMillan−Rowell oscillations which follow the equation, $\Delta V = n \times \frac{h v_F}{4 e d_s}$. Blue and red points are experimental data extracted from the positive and negative bias voltages, respectively. (f) Temperature dependence of differential conductance for various temperatures.

various crystal facets (see Figure 2a and d). The first type of NS junction is a standard lithographically defined contact that drapes over the edge of the exfoliated flake. This contact will form a junction with the [001] and [100] surfaces as well as the hinge between them. The second type of contact is fabricated by first transferring hexagonal boron nitride (hBN) over half of the FTS flake, insulating the side and edge from electrical contact. We then drape a contact over the side of the hBN, forming a junction primarily on the [001] face (see the depiction of the side view in Figure 2d). The entire fabrication process, from exfoliation to device, is performed in an inert argon atmosphere or vacuum. Patterns for mesoscale contacts were defined using standard photolithography techniques and our Heidelberg μPG101 direct-write lithography system. Contact areas are then cleaned with an argon plasma at high vacuum immediately before thermal deposition of 5 nm of Cr and then 45 nm of Au. Full fabrication details can be found in the Supporting Information.

Results and Discussion. We first established that our control contacts are only tunneling into the *c*-axis by studying their base temperature differential conductance. Specifically, we sourced current between a top contact (#5 or #6 in Figure 2a) to one of the current leads (#1 or #4), while measuring the resulting voltage between the same top contact and the other current contact. This three-point experiment ensures the conductance results primarily from the interface of the top contact. As shown in Figure 2b, we observe a small zero bias conductance peak that is ∼20% higher than the background. The shape and height are consistent with previous point contact Andreev reflection measurements along the *c*-axis of $FeTe_{0.55}Se_{0.45}$[46] and confirm the contacts are in the low bias, Andreev regime. We note these previous works were performed at temperatures below our base temperature and as such could resolve the rather small gap. At higher bias, we observe an enhancement in the conductance at $|V| \geq 20$ meV, consistent with the spin−orbit induced gap. Above this value, we observe a series of conductance dips that are fully consistent with McMillan−Rowell oscillations (MROs).[47,48] These MROs result from Fabry−Perot-like interference of quasiparticles in the normal layer undergoing AR at the interface and reflecting off the back surface of the metal. The MROs are linearly spaced by voltages[47] defined by the equation $\Delta(V) = n \cdot \frac{e v_F}{h d}$, where n is the dip number, v_F is the Fermi velocity at the contact, and d is the thickness of the metal which we set to 50 nm (see Figure 2e). From this fit, we extract a renormalized Fermi velocity of approximately 1.7×10^5 m/s. We note that similar behavior was observed if the current/voltage was reversed between contacts #1 and #4, we measure from contact #6, or we measure between contacts #6 and #5 exclusively (see Figure S4a). This shows the robustness of these results and, combined with the detailed spectra, confirms the contacts over the hBN are Andreev tunneling only into the *c*-axis.

Next, we turn to the spectra measured in an identical manner but with the hinge contact (#3 in Figure 2a). Since the normal state and high bias resistance of the hinge contact are nearly identical to the control contact, we expect the spectra to be similar. However, as shown in Figure 2c, the zero bias conductance in the hinge contact is quite distinct from the response observed in the control contact and previous point contact experiments. Specifically, we observe a cusp-like zero bias conductance peak (ZBCP) in the hinge contact that reaches a value 17 times higher than the high bias or $T \approx T_c$ conductance. This rather large enhancement is also likely responsible for the absence of a clear observation of the gap, which would be far smaller. These results provide strong

DOI: 10.1021/acs.nanolett.9b00844
Nano Lett. XXXX, XXX, XXX−XXX

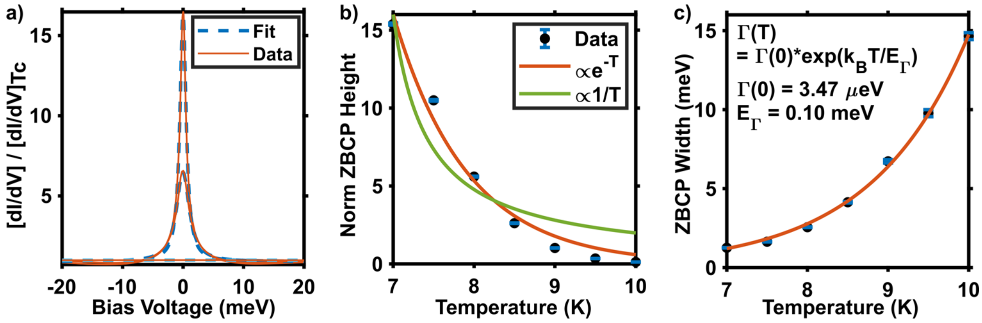

Figure 3. (a) dI/dV versus voltage normalized to the spectra taken at T_c (solid line) with a Lorentzian fit (dashed line), for $T = 7$, 9, and 15 K. (b and c) ZBCP heights and widths, respectively, extracted from the Lorentzian fit versus temperature. The exponential temperature dependence (orange lines) is at odds with a normal Andreev bound state that follows a $1/T$ dependence. The small energy scale of the exponential may result from the reduced superconducting gap on the side surfaces. The rather small width at zero temperature is consistent with a topologically protected 1D mode.

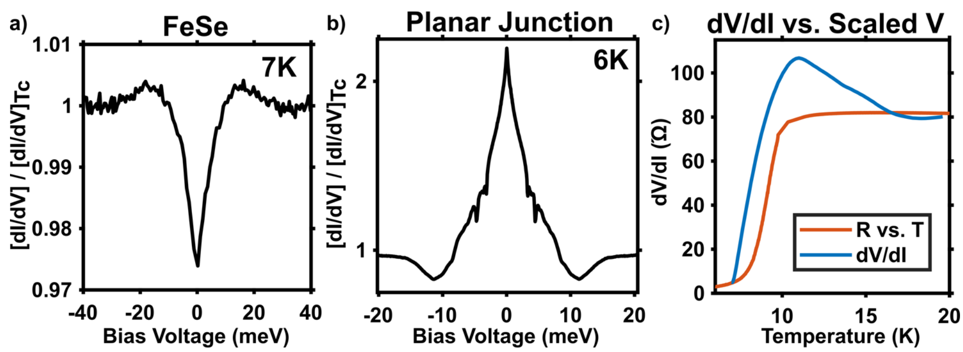

Figure 4. (a) Soft-point contact on a bulk crystal of FeSe normalized to the critical temperature. (b) Differential conductance using a planar junction, revealing a similar zero bias peak. The smaller height results from the normal resistance of the $Bi_2Te_2Se_1$ that is in series with the tunnel contact. (c) Differential resistance versus scaled voltage (blue) plotted along with the resistance versus temperature curve (orange). The strong overshoot of the voltage-dependent resistance and its return at high bias to the normal state resistance confirm the spectra and zero bias conductance peak are not a result of heating.

evidence for a zero mode that only exists on the hinge. The "cusp-like" shape and magnitude of the peak could result from an Andreev bound state (ABS);[39,41,42] however, this requires either a node in the superconducting gap or time-reversal symmetry breaking,[49,50] neither of which has been detected in $FeTe_{0.55}Se_{0.45}$.[25−27,30,32−34] As discussed later, direct evidence against the ABS interpretation is provided by the dependence of the peak on temperature and near independence on the contact's type (planar, point contact) or material (Ag, Au, $Bi_2Te_2Se_1$). Interestingly, this behavior is also inconsistent with previous observations of standard Andreev reflection (AR),[40] coherent Andreev reflection (CAR),[51] the Kondo effect,[52,53] and Joule heating.[54]

To ensure the zero bias conductance peak emerges at T_c and is not the result of an ABS, we directly analyzed its temperature dependence by fitting the data with a Lorentzian line shape. This is based on recent theoretical studies on one-dimensional superconducting wires showing that both Majorana zero modes and ABS produce Lorentzian differential conductance spectra.[44] While this may not be the correct model for our case, to the best of our knowledge, there are no calculations for the conductance spectra expected from hinge modes in a higher order topological superconductor. Nonetheless, the differential conductance spectra are generally well described by a Lorentzian (see Figure 3a). The temperature dependence of the height and width of the peak determined by the fits for the data presented in Figure 2f are shown in parts b and c of Figure 3, respectively. These data provide direct evidence for the connection to the bulk superconductivity, though they are inconsistent with an ABS. Indeed, we find that, as the temperature is raised, the height of the ZBCP decreases exponentially until it is completely quenched at T_c (see Figure 2a and Figure 3b), where we define T_c as the temperature for which $\frac{dR}{dT}$ passes through zero. While lower temperature data are required to determine the exact functional form, it is clear from Figure 3b and c that the mode is substantially different from the $1/T$ behavior typically expected from an ABS. Furthermore, we found a similar shape and temperature dependence in contacts of various barrier height, also inconsistent with standard Andreev reflection.[19,55,56]

Similar to the height of the peak, we find the width of the zero bias conductance peak grows exponentially with temperature (see Figure 3). Interestingly, the energy scales governing the peak height ($E_H \approx 0.08$ meV) and the width ($E_\Gamma \approx 0.1$ meV) are quite close. We note that comparable results were obtained from other contacts revealing the hinge mode. Nonetheless, the energy scales governing the temperature dependence of the mode are far smaller than either the superconducting gap of the bulk or the surface states.[20] However, to the best of our knowledge, the size of the superconducting gap on the side surface has not been measured. As such, we speculate this small apparent energy scale results from a much weaker proximity effect on the [010] and [100] surface states. Interestingly, extrapolating the width of the zero bias peak to zero temperature suggests an extremely

DOI: 10.1021/acs.nanolett.9b00844
Nano Lett. XXXX, XXX, XXX−XXX

narrow mode (≈3.5 μeV). While further studies at lower temperatures are required to confirm this extrapolation and the specific shape of the mode, if correct, it points to the highly coherent nature of the excitation. As such, the temperature dependence is consistent with our expectations for topologically protected 1D modes.

For additional confirmation that the ZBCP does not result from fabrication, exfoliation, impurities, or the specific metal used in the contact, we performed a series of additional control experiments, summarized in Figure 4. First, the topological gap in FTS closes with reduced tellurium levels; thus, we expect the hinge mode is absent from FeSe. To confirm this as well as the irrelevance of contact type or normal metal used, we employed soft-point contact measurements. For FeSe, we observe no evidence of an increase in conductance at zero bias below T_c (see Figure 4a). However, performing the same soft-point contact spectroscopy across multiple different $FeTe_{0.55}Se_{0.45}$ crystals always produces an increase in conductance at zero bias when cooled below T_c consistent with the data on contacts made via photolithography (see Figure S3). The soft-point contacts revealed a smaller enhancement of the zero bias conductance in the superconducting state. However, this is expected, since the quasi-particle lifetime in the Ag paint contact is likely lower, which smears the spectra and reduces the height at zero bias. Similarly, we used planar junctions with $Bi_2Te_2Se_1$ via a method that has previously enabled spectroscopic studies with low barriers in van der Waals materials.[15] As shown in Figure 4b, these junctions also resulted in nearly identical spectra near zero bias. Here the lower zero bias conductance is expected, as it contains contributions from the normal material being in series with the contact. Another extrinsic explanation for the peak is the interstitial Fe atoms known to be present in these materials. However, we excluded this explanation by measurements on annealed samples where the Fe impurity content is dramatically reduced (see Figure S3a), though the topology and T_c are only mildly affected.

An alternate mechanism for producing a ZBCP is Joule heating at the contact. We took a number of steps to rule this out. First, similar results were obtained regardless of the exact contact configuration (e.g., swapping contacts employed for current versus voltage in point contact or three-point measurements). In addition, we compared the voltage and temperature data by inverting the $\frac{dI}{dV}$ spectra and comparing them to the resistance versus temperature data taken on the same contact configuration (see Figure 4c). To align the two curves, we translate the $\frac{dV}{dI}$ curve such that zero voltage coincides with the temperature at which it was recorded (7 K). Next, we assume the voltage where the maximum resistance is measured is equivalent to heating to T_c, as this is the temperature where a peak in resistance is typically observed (see Figure 1d). While the exact voltage dependence due to heating could be more complex, it is clear the $\frac{dV}{dI}$ versus voltage spectra are far in excess of the resistance measured at T_c, though at high bias they do return to the value measured at T_c. This further excludes voltage induced heating as the origin of the zero bias conductance peak. In addition, the background conductances in the *c*-axis, hinge, and point contacts are nearly identical. Therefore, the heating across all of them should be approximately the same. However, they reveal quite distinct spectra (i.e., strong ZBCP in the hinge contact vs nearly none in the *c*-axis) which, combined with the emergence of the zero bias conductance peak (ZBCP) at T_c in numerous contacts (see Figure 2 and Figure S2), eliminates heating.

In summary, via a variety of contact methods, we reveal helical hinge zero modes in the topological superconductor $FeTe_{0.55}Se_{0.45}$. Specifically, contacts to the [001] surface made using hBN reveal standard Andreev reflection, while those draped over the hinge contain a cusp-like, zero energy feature in the differential conductance. By combining with measurements using soft-point contacts on various crystals, we further confirm the intrinsic nature of this new mode. Furthermore, the appearance of an HHZM in FTS helps to establish both the topological and $s^{\pm}$ nature of the superconductivity. An important question raised by these results is the large size and the temperature dependence of the HHZM. It is possible that the large ratio of contact area to coherence length at the measured temperature (≈1000*x*), makes the measurement essentially many point-like contacts in parallel, leading to an apparently large conductance. The contact size may also play a role in the temperature dependence, as could the unknown size of the superconducting gap on the side surface. Thus, future theoretical and experimental efforts must be made to better separate out the contact effects from the intrinsic response of the hinge mode we observe.

■ ASSOCIATED CONTENT

Supporting Information

The Supporting Information is available free of charge on the ACS Publications website at DOI: 10.1021/acs.nanolett.9b00844.

> Details regarding exfoliation and fabrication of devices, the experimental measurement setup, additional crystal measurements, and additional controls and checks performed on the devices (PDF)

■ AUTHOR INFORMATION

Corresponding Author

*E-mail: ks.burch@bc.com.

ORCID

Mason J. Gray: 0000-0002-2778-9166

Notes

The authors declare no competing financial interest.

■ ACKNOWLEDGMENTS

K.S.B., R.O., and M.J.G. acknowledge support from the National Science Foundation, Award No. DMR-1709987. Work at Brookhaven National Laboratory was supported by the Office of Science, U.S. Department of Energy, under Contract No. DE-SC0012704. Growth of hexagonal boron nitride crystals was supported by the Elemental Strategy Initiative conducted by the MEXT, Japan, and the CREST (JPMJCR15F3), JST. We are grateful for numerous discussions with V. Yakovenko, V. Galitski, K. T. Law, R.-X. Zhang, W. Cole, K. Jiang, and Z. Wang.

■ REFERENCES

(1) Balents, L. Spin liquids in frustrated magnets. *Nature* **2010**, *464*, 199–208.

(2) Armitage, N. P.; Mele, E. J.; Vishwanath, A. Weyl and Dirac Semimetals in Three Dimensional Solids. *Rev. Mod. Phys.* **2018**, *90*, No. 015001.

(3) Zhang, C.; Zhang, Y.; Yuan, X.; Lu, S.; Zhang, J.; Narayan, A.; Liu, Y.; Zhang, H.; Ni, Z.; Liu, R.; et al. Quantum Hall effect based on Weyl orbits in Cd3As2. *Nature* **2019**, *565*, 331−336.

(4) Nayak, C.; Simon, S. H.; Stern, A.; Freedman, M.; Das Sarma, S. Non-Abelian anyons and topological quantum computation. *Rev. Mod. Phys.* **2008**, *80*, 1083−1159.

(5) Schindler, F.; Wang, Z.; Vergniory, M. G.; Cook, A. M.; Murani, A.; Sengupta, S.; Kasumov, A. Y.; Deblock, R.; Jeon, S.; Drozdov, I.; et al. Higher-order topology in bismuth. *Nat. Phys.* **2018**, *14*, 918−924.

(6) Ni, X.; Weiner, M.; Alù, A.; Khanikaev, A. B. Observation of higher-order topological acoustic states protected by generalized chiral symmetry. *Nat. Mater.* **2019**, *18*, 113.

(7) Xue, H.; Yang, Y.; Gao, F.; Chong, Y.; Zhang, B. Acoustic higher-order topological insulator on a kagome lattice. *Nat. Mater.* **2019**, *18*, 108−112.

(8) Song, Z.; Fang, Z.; Fang, C. (d-2) -Dimensional Edge States of Rotation Symmetry Protected Topological States. *Phys. Rev. Lett.* **2017**, *119*, 1−5.

(9) Langbehn, J.; Peng, Y.; Trifunovic, L.; Von Oppen, F.; Brouwer, P. W. Reflection-Symmetric Second-Order Topological Insulators and Superconductors. *Phys. Rev. Lett.* **2017**, *119*, 1−5.

(10) Benalcazar, W. A.; Bernevig, B. A.; Hughes, T. L. Quantized electric multipole insulators. *Science* **2017**, *357*, 61−66.

(11) Wang, Q.; Liu, C.-c.; Lu, Y.-m.; Zhang, F. High-Temperature Majorana Corner States. *Phys. Rev. Lett.* **2018**, *121*, 186801.

(12) Zhang, R.-X.; Cole, W. S.; Sarma, S. D. Helical Hinge Majoranas in Iron-Based Superconductors. *Phys. Rev. Lett.* **2019**, *122*, 187001.

(13) Yan, Z.; Song, F.; Wang, Z. Majorana Corner Modes in a High-Temperature Platform. *Phys. Rev. Lett.* **2018**, *121*, No. 096803.

(14) Ghorashi, S. A. A.; Hu, X.; Hughes, T. L.; Rossi, E. Second-order Dirac superconductors and magnetic field induced Majorana hinge modes. *arXiv e-prints* **2019**, arXiv:1901.07579.

(15) Zareapour, P.; Hayat, A.; Zhao, S. Y. F.; Kreshchuk, M.; Jain, A.; Kowk, D. C.; Lee, N.; Cheong, S.-W.; Xu, Z.; Yang, A.; et al. Proximity-induced high-temperature superconductivity in the topological insulators Bi2Se3 and Bi2Te3. *Nat. Commun.* **2012**, *3*, 1056.

(16) Albrecht, S.; Higginbotham, A.; Madsen, M.; Kuemmeth, F.; Jespersen, T.; Nygård, J.; Krogstrup, P.; Marcus, C. Exponential protection of zero modes in Majorana islands. *Nature* **2016**, *531*, 206−209.

(17) Gazibegovic, S.; Car, D.; Zhang, H.; Balk, S. C.; Logan, J. A.; de Moor, M. W. A.; Cassidy, M. C.; Schmits, R.; Xu, D.; Wang, G.; et al. Epitaxy of advanced nanowire quantum devices. *Nature* **2017**, *548*, 434−438.

(18) Kurter, C.; Finck, A. D. K.; Huemiller, E. D.; Medvedeva, J.; Weis, A.; Atkinson, J. M.; Qiu, Y.; Shen, L.; Lee, S. H.; Vojta, T. Conductance Spectroscopy of Exfoliated Thin Flakes of $Nb_xBi_2Se_3$. *Nano Lett.* **2019**, *19*, 38−45.

(19) Tanaka, Y.; Sato, M.; Nagaosa, N. Symmetry and Topology in Superconductors − Odd-Frequency Pairing and Edge States−. *J. Phys. Soc. Jpn.* **2012**, *81*, No. 011013.

(20) Zhang, P.; Yaji, K.; Hashimoto, T.; Ota, Y.; Kondo, T.; Okazaki, K.; Wang, Z.; Wen, J.; Gu, G. D.; Ding, H.; et al. Observation of topological superconductivity on the surface of an iron-based superconductor. *Science* **2018**, *360*, 182−186.

(21) Wang, Z.; Zhang, P.; Xu, G.; Zeng, L. K.; Miao, H.; Xu, X.; Qian, T.; Weng, H.; Richard, P.; Fedorov, A. V.; et al. Topological nature of the $FeSe_{0.5}Te_{0.5}$ superconductor. *Phys. Rev. B: Condens. Matter Mater. Phys.* **2015**, *92*, 115119.

(22) Wang, D.; Kong, L.; Fan, P.; Chen, H.; Zhu, S.; Liu, W.; Cao, L.; Sun, Y.; Du, S.; Schneeloch, J.; et al. Evidence for Majorana bound states in an iron-based superconductor. *Science* **2018**, *362*, 333−335.

(23) Liu, T. J.; Hu, J.; Qian, B.; Fobes, D.; Mao, Z. Q.; Bao, W.; Reehuis, M.; Kimber, S. A. J.; Prokes, K.; Matas, S.; et al. From (p,0) magnetic order to superconductivity with (p,p) magnetic resonance in Fe1.02Te1-xSex. *Nat. Mater.* **2010**, *9*, 718.

(24) Homes, C. C.; Dai, Y. M.; Wen, J. S.; Xu, Z. J.; Gu, G. D. FeTe $ _{0.55}Se_{0.45}$: A multiband superconductor in the clean and dirty limit. *Phys. Rev. B: Condens. Matter Mater. Phys.* **2015**, *91*, 144503.

(25) Hanaguri, T.; Niitaka, S.; Kuroki, K.; Takagi, H. Unconventional s-Wave Superconductivity in Fe(Se,Te). *Science* **2010**, *328*, 474−476.

(26) Miao, H.; Richard, P.; Tanaka, Y.; Nakayama, K.; Qian, T.; Umezawa, K.; Sato, T.; Xu, Y. M.; Shi, Y. B.; Xu, N. Isotropic superconducting gaps with enhanced pairing on electron Fermi surfaces in FeTe0.55Se0.45. *Phys. Rev. B: Condens. Matter Mater. Phys.* **2012**, *85*, No. 094506.

(27) Okazaki, K.; Ito, Y.; Ota, Y.; Kotani, Y.; Shimojima, T.; Kiss, T.; Watanabe, S.; Chen, C. T.; Niitaka, S.; Hanaguri, T. Evidence for a cos (4ϕ) modulation of the superconducting energy gap of optimally doped FeTe0.6Se0.4 single crystals using laser angle-resolved photoemission spectroscopy. *Phys. Rev. Lett.* **2012**, *109*, 237011.

(28) Kreisel, A.; Andersen, B. M.; Sprau, P. O.; Kostin, A.; Séamus Davis, J. C.; Hirschfeld, P. J. Orbital selective pairing and gap structures of iron-based superconductors. 2016, arXiv:1611.02643. arXiv.org e-Print archive. https://arxiv.org/abs/1611.02643.

(29) Chubukov, A. Pairing Mechanism in Fe-Based Superconductors. *Annu. Rev. Condens. Matter Phys.* **2012**, *3*, 57−92.

(30) Zeng, B.; Mu, G.; Luo, H. Q.; Xiang, T.; Mazin, I. I.; Yang, H.; Shan, L.; Ren, C.; Dai, P. C.; Wen, H. H. Anisotropic structure of the order parameter in FeSe0.45Te0.55revealed by angle-resolved specific heat. *Nat. Commun.* **2010**, *1*, No. 112.

(31) Michioka, C.; Ohta, H.; Matsui, M.; Yang, J.; Yoshimura, K.; Fang, M. Macroscopic physical properties and spin dynamics in the layered superconductor Fe1+δTe1-xSex. *Phys. Rev. B: Condens. Matter Mater. Phys.* **2010**, *82*, 1−7.

(32) Serafin, A.; Coldea, A. I.; Ganin, A. Y.; Rosseinsky, M. J.; Prassides, K.; Vignolles, D.; Carrington, A. Anisotropic fluctuations and quasiparticle excitations in FeSe 0.5 Te0.5. *Phys. Rev. B: Condens. Matter Mater. Phys.* **2010**, *82*, 1−9.

(33) Bendele, M.; Weyeneth, S.; Puzniak, R.; Maisuradze, A.; Pomjakushina, E.; Conder, K.; Pomjakushin, V.; Luetkens, H.; Katrych, S.; Wisniewski, A.; et al. Anisotropic superconducting properties of single-crystalline FeSe0.5Te0.5. *Phys. Rev. B: Condens. Matter Mater. Phys.* **2010**, *81*, 1−10.

(34) Kim, H.; Martin, C.; Gordon, R. T.; Tanatar, M. A.; Hu, J.; Qian, B.; Mao, Z. Q.; Hu, R.; Petrovic, C.; Salovich, N.; et al. London penetration depth and superfluid density of single-crystalline Fe1+y (Te1-x Sex) and Fe1+y (Te1-x Sx). *Phys. Rev. B: Condens. Matter Mater. Phys.* **2010**, *81*, 3−6.

(35) Chen, Y. L.; Analytis, J. G.; Chu, J.-H.; Liu, Z. K.; Mo, S.-K.; Qi, X. L.; Zhang, H. J.; Lu, D. H.; Dai, X.; Fang, Z.; et al. Experimental Realization of a Three-Dimensional Topological Insulator, Bi2Te3. *Science* **2009**, *325*, 178−181.

(36) Zhang, P.; Wang, Z.; Wu, X.; Yaji, K.; Ishida, Y.; Kohama, Y.; Dai, G.; Sun, Y.; Bareille, C.; Kuroda, K.; et al. Multiple topological states in iron-based superconductors. *Nat. Phys.* **2019**, *15*, 41−47.

(37) Liu, Q.; Chen, C.; Zhang, T.; Peng, R.; Yan, Y. J.; Wen, C. H. P.; Lou, X.; Huang, Y. L.; Tian, J. P.; Dong, X. L. Robust and Clean Majorana Zero Mode in the Vortex Core of High-Temperature Superconductor $(Li_{0.84}Fe_{0.16})$OHFeSe. *Phys. Rev. X* **2018**, *8*, No. 041056.

(38) Machida, T.; Sun, Y.; Pyon, S.; Takeda, S.; Kohsaka, Y.; Hanaguri, T.; Sasagawa, T.; Tamegai, T. Zero-energy vortex bound state in the superconducting topological surface state of Fe(Se,Te). 2018, arXiv:1812.08995. arXiv.org e-Print archive. https://arxiv.org/abs/1812.08995.

(39) Deutscher, G. Andreev−Saint-James reflections: A probe of cuprate superconductors. *Rev. Mod. Phys.* **2005**, *77*, 109−135.

(40) Tanaka, Y.; Tanuma, Y.; Kuroki, K.; Kashiwaya, S. Doppler shift of zero energy Andreev bound state. *Phys. B* **2003**, *329*−*333*, 1444−1445.

DOI: 10.1021/acs.nanolett.9b00844
Nano Lett. XXXX, XXX, XXX−XXX

(41) Sinha, S.; Ng, K.-W. Zero Bias Conductance Peak Enhancement in $Bi_2Sr_2CaCu_2O_8$/Pb Tunneling Junctions. *Phys. Rev. Lett.* **1998**, *80*, 1296−1299.
(42) Aprili, M.; Badica, E.; Greene, L. H. Doppler Shift of the Andreev Bound States at the YBCO Surface. *Phys. Rev. Lett.* **1999**, *83*, 4630−4633.
(43) Zhang, Y.-T.; Hou, Z.; Xie, X. C.; Sun, Q.-F. Quantum perfect crossed Andreev reflection in top-gated quantum anomalous Hall insulator−superconductor junctions. *Phys. Rev. B: Condens. Matter Mater. Phys.* **2017**, *95*, 245433.
(44) Setiawan, F.; Liu, C.-X.; Sau, J. D.; Das Sarma, S. Electron temperature and tunnel coupling dependence of zero-bias and almost-zero-bias conductance peaks in Majorana nanowires. *Phys. Rev. B: Condens. Matter Mater. Phys.* **2017**, *96*, 184520.
(45) Park, W. K.; Hunt, C. R.; Arham, H. Z.; Xu, Z. J.; Wen, J. S.; Lin, Z. W.; Li, Q.; Gu, G. D.; Greene, L. H. Strong Coupling Superconductivity in Iron-Chalcogenide $FeTe_{0.55}Se_{0.45}$. 2010, arXiv:1005.0190. arXiv.org e-Print archive. https://arxiv.org/abs/1005.0190.
(46) Daghero, D.; Pecchio, P.; Ummarino, G. A.; Nabeshima, F.; Imai, Y.; Maeda, A.; Tsukada, I.; Komiya, S.; Gonnelli, R. S. Point-contact Andreev-reflection spectroscopy in Fe(Te,Se) films: multi-band superconductivity and electron-boson coupling. *Supercond. Sci. Technol.* **2014**, *27*, 124014.
(47) Chang, H.-S.; Bae, M.-H.; Lee, H.-J. McMillan-Rowell oscillations observed in c-axis Au/Bi2Sr2CaCu2O8+δ junctions. *Phys. C* **2004**, *408*, 618−619.
(48) Shkedy, L.; Aronov, P.; Koren, G.; Polturak, E. Observation of McMillan-Rowell like oscillations in underdoped YBa2Cu3Oy junctions oriented along the node of the d-wave order parameter. *Phys. Rev. B: Condens. Matter Mater. Phys.* **2004**, *69*, 132507.
(49) Sengupta, K.; Kwon, H.-J.; Yakovenko, V. M. Edge states and determination of pairing symmetry in superconducting Sr_2RuO_4. *Phys. Rev. B: Condens. Matter Mater. Phys.* **2002**, *65*, 104504.
(50) Tanaka, Y.; Sato, M.; Nagaosa, N. Symmetry and Topology in Superconductors − Odd-Frequency Pairing and Edge States−. *J. Phys. Soc. Jpn.* **2012**, *81*, No. 011013.
(51) van Wees, B. J.; de Vries, P.; Magnée, P.; Klapwijk, T. M. Excess conductance of superconductor-semiconductor interfaces due to phase conjugation between electrons and holes. *Phys. Rev. Lett.* **1992**, *69*, 510−513.
(52) Sasaki, S.; De Franceschi, S.; Elzerman, J. M.; van der Wiel, W. G.; Eto, M.; Tarucha, S.; Kouwenhoven, L. P. Kondo effect in an integer-spin quantum dot. *Nature* **2000**, *405*, 764.
(53) Samokhin, K. V.; Walker, M. B. Effect of magnetic field on impurity bound states in high-T_c superconductors. *Phys. Rev. B: Condens. Matter Mater. Phys.* **2001**, *64*, No. 024507.
(54) Naidyuk, Y.; Kvitnitskaya, O.; Bashlakov, D.; Aswartham, S.; Morozov, I.; Chernyavskii, I.; Fuchs, G.; Drechsler, S.-L.; Hühne, R.; Nielsch, K.; et al. Surface superconductivity in the Weyl semimetal MoTe2 detected by point contact spectroscopy. *2D Mater.* **2018**, *5*, No. 045014.
(55) Blonder, G. E.; Tinkham, M.; Klapwijk, T. M. Transition from metallic to tunneling regimes in superconducting microconstrictions: Excess current, charge imbalance, and supercurrent conversion. *Phys. Rev. B: Condens. Matter Mater. Phys.* **1982**, *25*, 4515−4532.
(56) Löfwander, T.; Shumeiko, V. S.; Wendin, G. TOPICAL REVIEW: Andreev bound states in high-T_c superconducting junctions. *Supercond. Sci. Technol.* **2001**, *14*, R53−R77.

DOI: 10.1021/acs.nanolett.9b00844
Nano Lett. XXXX, XXX, XXX−XXX